Accepted Manuscript

Quantifying the contributions of various emission sources to black carbon and assessment of control strategies in western China

Junhua Yang, Shichang Kang, Deliang Chen, Zhenming Ji, Lekhendra Tripathee, Xintong Chen, Wentao Du, Guiqiang Qiu

PII: S0169-8095(18)30516-7
DOI: doi:10.1016/j.atmosres.2018.09.003
Reference: ATMOS 4362

To appear in: *Atmospheric Research*

Received date: 23 April 2018
Revised date: 15 August 2018
Accepted date: 5 September 2018

Please cite this article as: Junhua Yang, Shichang Kang, Deliang Chen, Zhenming Ji, Lekhendra Tripathee, Xintong Chen, Wentao Du, Guiqiang Qiu , Quantifying the contributions of various emission sources to black carbon and assessment of control strategies in western China. Atmos (2018), doi:10.1016/j.atmosres.2018.09.003

Quantifying the contributions of various emission sources to black carbon and assessment of control strategies in western China

Junhua Yang[1], Shichang Kang[1,2,*] shichang.kang@lzb.ac.cn, Deliang Chen[2,3], Zhenming Ji[4,*] jizhm3@mail.sysu.edu.cn, Lekhendra Tripathee[1], Xintong Chen[1], Wentao Du[1], Guiqiang Qiu[5]

[1]State Key Laboratory of Cryospheric Sciences, Northwest Institute of Eco-Environment and Resources, Chinese Academy of Sciences (CAS), Lanzhou,730000

[2]CAS Center for Excellence in Tibetan Plateau Earth Sciences, Beijing, 100101

[3]Regional Climate Group, Department of Earth Sciences, University of Gothenburg, Gothenburg, Sweden, 40530

[4]School of Atmospheric Sciences, and Guangdong Province Key Laboratory for Climate Change and Natural Disaster Studies, Sun Yat-sen University, Guangzhou, 510275

[5]Shanxi Meteorological Observatory, Taiyuan, 030006

[*]Corresponding authors.

Abstract

In this study, an air quality model WRF-Chem (Weather Research and Forecasting Chemical) was used to simulate meteorological conditions and surface black carbon (BC) concentrations in the western China from June 2016 to May 2017, given emissions from various sources in Asia. Comparison between simulations and measurements in western China showed that the model can capture the key spatial and temporal features of meteorological elements and surface BC concentrations. The modeling framework was then used to quantify the relative contributions of different emission sectors to BC concentrations via sensitivity experiments. Our results show that the residential emission sector presented the largest contribution in western China. The second largest contributor for the highly populated mega-cities (HM) region including Sichuan and Guanzhong basins, and for the remote background (RB) region covering the central part of the Tibetan Plateau (TP), was the industrial sector and the transportation sector, respectively. Power plants and open biomass burning sources played minor roles in the regional BC concentration. The seasonality of BC concentrations showed higher values in winter, mainly due to the residential winter heating under conditions of lower precipitation scavenging and poor boundary layer mixing. A further evaluation of emission control strategies shows that a 50% reduction of residential emissions caused annual mean surface BC concentrations in the RB and HM regions to decrease by 36.2% and 36.7%, respectively. In contrast, a 50% reduction in industrial emissions or transportation emissions led to less than 12%

decreases in both regions. The 50% reduction of transportation emissions caused BC concentrations to decrease by 9.2% in the RB region, larger than the 5.9% decrease caused by a 50% reduction of industrial emissions. Transportation emissions were responsible for more BC pollution than industrial emissions for the RB region, in contrast to the highly-industrialized HM region. Therefore, more attention should be paid to transportation emissions when designing control strategies for air pollution over the TP. The results from this work provide useful information for local governments to prepare and implement air pollution guidelines in western China.

Keywords: black carbon, emission sources in Asia, Tibetan Plateau, highly populated region, control strategies.

1. Introduction

Black carbon (BC), also known as elemental carbon, is produced by incomplete combustion of carbonaceous material, mainly fossil fuels (e.g., diesel, coal) and biomass (e.g., biofuel, agricultural and forest fires). BC has a potential to warm the atmosphere and cool the surface by absorbing solar radiation (Ramanathan et al., 2007), and furthermore modify atmospheric circulation pattern (Lau et al., 2010; Bond et al., 2013). When deposited on snow/ice surface, it can also reduce the albedo (Hansen et al., 2004; Flanner et al., 2007; Ji et al., 2016a, b) and enhance the glacier melt (Kang et al., 2016; Chen et al., 2015; Li et al., 2018; Zhang et al., 2017). The fifth assessment report of the Intergovernmental Panel on Climate Change (IPCC) indicates that BC from biofuel and fossil fuel led to a direct radiative forcing of around +0.4 W m^{-2} (Boucher et al., 2013). In addition to its impact on the climate system, BC can also adversely affect air quality because of its contribution to regional haze and poor visibility (Cao et al., 2012). Furthermore, BC is a strong absorbent of various toxic chemicals and can cause deleterious impacts on human health (Dachs et al., 2000; Anenberg et al., 2012). Therefore, reduction of BC emission can lead to the dual benefits of combating global warming and improving human health.

Many efforts have been made to estimate BC emissions in China. Streets et al. (2000) concluded that China's BC emissions for the year 2000 were 1.05 Tg. Using a technology-based approach, Lei et al. (2011) developed an inventory of anthropogenic emissions in China for 1990-2005 which indicates no significant trends of BC until 2000, but an increase after 2000 with the peaks of BC (1.51 Tg) in 2005. By a series

of improved methodologies, Zhang et al. (2009) estimated China's anthropogenic BC emission to be 1.8 Tg in the year 2006. Later on, Lu et al. (2011) developed a new inventory of BC emission for China from the period of 1996~2010, inferring an increase in BC emissions by 46 % from 1.27 Tg in the year 2000 to 1.85 Tg in the year 2010. In general, the annual mean BC emissions in China continuously increased in the first decade of the 21st century.

Previous studies have assessed the regional and seasonal variation of the BC sources in China, mainly based on emission inventory data. The MIX emission inventory shows that residential sectors contributed to more than 60% of annual total BC emission due to abounding home heating in Northern China (Li et al., 2017b). Meanwhile, in southern China, industrial sources dominated from spring to autumn, contributing to around 50% of annual total BC emission in Yangtze River Delta region (Zhang et al., 2009; Li et al., 2015). The transportation sector played the most important role for BC emission (65%) in the Pearl River Delta region, as calculated from a high-resolution regional BC emission inventory (Zheng et al., 2012). However, there are limited studies on model-based characterizations of source contributions to BC in China. Chemical transport models can reveal the relationship between the emission sources and ambient concentrations, and provide assessment of control strategies.

Relatively few studies on BC source apportionment have been reported in western China. Using source-diagnostic $\Delta^{14}C/\delta^{13}C$ isotopic ratios from several sites mainly located in southern TP, Li et al. (2016a) found almost equal contributions to

BC aerosol from fossil fuel (46±11%) and biomass (54±11%) combustion. However, owing to the harsh environment of western China, which has resulted in limited access for fieldwork, and a sparsity of fixed instrumental stations, observational records are too poor to enable detailed, quantitative studies of the spatial and temporal trends of BC in the TP. The Advanced Weather Research and Forecasting (WRF-ARW) model (Skamarock et al., 2005) with Chemistry (WRF-Chem), is a regional chemistry model that has been used to quantify the contributions of different emission sources to BC concentration in western China. One such study examined total BC concentrations in the highly populated mega-cities of the Guanzhong basin, western China from May 2013 to April 2014, and found that residential sources contributed the most to BC concentration, followed by industrial and transportation sectors (Li et al., 2016b). Model-based emission source characterizations of BC concentrations in the more remote regions of western China like the TP are still scarce. To the best of our knowledge, this is the first study using the WRF-Chem model to preform source apportion of BC and assess emission control strategies for BC over the TP.

In this study, one year of WRF-Chem simulation was conducted covering the period from June 2016 to May 2017. Furthermore, we calculated the sectoral contributions to BC concentrations and assessed the corresponding emission sources and control strategies in western China. Four main anthropogenic emission sectors (residential, industrial, power generation and transportation), as well as open biomass combustion source, were considered here. This work also aims to provide a baseline

to formulate control strategies of the atmospheric pollutants for policy makers.

2. Model and data

2.1. WRF-Chem model and experimental setup

The regional climate-chemistry model WRF-Chem is an online three-dimensional, Eulerian chemical transport model that considers complex physical and chemical processes, such as the dry and wet depositions, transport (advection, convective, and diffusion), gaseous and aqueous chemical transformation, aerosol chemistry and dynamics (Grell et al., 2005). It simulates gas-phase chemical and aerosol-microphysical processes on-line with the meteorological field and has been successfully used in air quality studies in China (Wang et al., 2014; Gao et al., 2015; Yang et al., 2017a, 2018). The WRF-Chem model used in this study was version 3.6.1. The Yonsei University (YSU) planetary boundary layer scheme was used, which uses counter-gradient terms to represent fluxes and considers the entrainment effect (Schaefer, 1990). The Morrison 2-moment microphysical parameterization (Morrison et al., 2007), the RRTMG longwave and shortwave radiation scheme (Zhao et al., 2011), and the Noah land surface (Chen and Dudhia, 2001) were utilized in this study. Based on our previous sensitivity experiments using chemical schemes (Yang et al., 2017b), the chemistry parameterization options were the Carbon Bond Mechanism Version Z (CBMZ; Zaveri and Peters, 1999) for gas-phase chemistry and the Model for Simulating Aerosol Interactions and Chemistry (MOSAIC; Zaveri et al., 2008) for aerosol reactions scheme.

As shown in Table 1, the original BC emission in the model was unchanged in

the base experiment. We conducted other five sensitivity experiments (S1, S2, S3, S4, and S5) by turning off each emission sectors (residential, industry, transportation, power and open biomass burning) in turn. The contribution of each emission sector to total BC concentrations can be estimated as the difference between the base and the specific sensitivity experiment. Additionally, we performed other three sensitivity experiments to assess emission control strategies to reduce BC pollution, by reducing industry, transportation BC emission sources to 50% successively. The WRF-Chem simulations in this study were performed at two nested computational domains. On a Mercator map (Fig. 1), the coarse domain (d01) contained 81 × 65 grid points with a 75-km spatial resolution, while the nested domain (d02) consisted of 147 × 112 grid points with a 25-km spatial resolution. The d02 domain covered large parts of western China, centered at 39°N, 92°E, and had 30 vertical layers with a model top pressure of 50 hPa. The National Centers for Environmental Prediction final analysis data (NCEP FNL), with a horizontal resolution of 1° × 1° at 6-h time intervals, provided initial and boundary conditions for the meteorological fields. The simulation was conducted for a period of one year, from May 2016 to May 2017. The first month of the simulation was considered as the model spin-up time and not analyzed.

To contrast the regional difference of the sectoral contributions to BC concentrations, we categorized the inner part of the TP as the remote background (RB) region with the blue box in Fig. 1, and categorized eastern Sichuan, Chongqing and southern Shaanxi as the high population and mega-cities (HM) region with the red box in Fig.1.

2.2. Emissions

The anthropogenic emissions were based on the multi-resolution emission inventory for China (MEIC, Li et al., 2017b) for the year 2010, and included residential, industry, transportation, power, as well as agriculture (only for NH_3) sources. The total annual anthropogenic BC emission calculated by the MEIC for Asia was 1.186 Mg/month, including 0.695 Mg/month from residential sources, 0.297 Mg/month from industry, 0.194 Mg/month from transportation, and 0.002 Mg/month from power generation, as presented in Fig. S1. Greenhouse gas emissions (e.g. CO_2, CH_4, and N_2O) were derived from the Reanalysis of the TROpospheric chemical composition (RETRO, http://retro.enes.org/index.shtml) with 0.5° × 0.5° resolution. The sea salt and volcanic ash emissions in the study domain were interpolated from a global emissions dataset (*Freitas et al*., 2011). The fire emissions inventory was based on the Fire INventory from NCAR (FINN) (Wiedinmyer et al., 2010). This inventory provides high spatial (1 km × 1 km) and temporal (daily) resolutions for emission estimation and includes agricultural fires, wildfire, and prescribed burning sources. The BC emission flux from the fire inventory in western China (domain d02) was much lower than that from the other anthropogenic emission sources (Fig. S2).

2.3. Data

In this study, a total of 273 national weather stations from the China Meteorological Data Network (CMDN, http://data.cma.cn) were used to evaluate the simulated surface temperature, precipitation, and surface wind. Fig. 1 represents the locations of these weather stations with black dots. Simulated surface air temperature

and wind fields at 500 hPa were validated against the ERA-Interim reanalysis data produced by the European Centre for Medium-Range Weather Forecasts (ECMWF, Dee et al. 2011, http://apps.ecmwf.int), with a resolution of 0.25°. Simulated precipitation was verified against precipitation from the Climate Research Unit (CRU, Mitchell and Jones, 2005, http://crudata.uea.ac.uk/cru), with a resolution of 0.5°. The identification of black carbon over the study area was based on the outputs from a chemical transport model MOZART (Model for OZone and Related chemical Tracers, http://www.acom.ucar.edu/wrf-chem/mozart.shtml, Emmons et al., 2010). Additionally, the near-surface BC concentrations at 7 sites from previous studies were incorporated for the validation of model performance. In this study, Xi'an, Lanzhou, and Urumqi are urban sites with highly populated areas. The other four sites are located in the remote areas of the TP.

3. Results and discussions

3.1. Model evaluation

3.1.1. Meteorology

This section compares the 2-m temperature (T2), precipitation, and wind at 500 hPa from the base simulation with the ERA-Interim dataset. WRF-Chem reproduced the spatial and temporal variation in T2 well against the ERA-Interim dataset (Fig. 2). The simulated surface air temperature was high as 12 °C in the TP during summer and as low as -12 °C during winter. Warmer regions surrounding the TP such as the east of Sichuan province and the south of Xinjiang province had surface air temperatures exceeding 24 °C during summer.

Fig. 3 shows the reanalysis and simulated mean wind at 500 hPa in summer and winter. The WRF-Chem mean wind fields were consistent with the ERA-Interim mean wind fields. During summer, southwesterly winds prevailed across the Himalayas, and westerly wind dominated north of 40°N (Fig. 3a and Fig. 3c). Strong westerly winds prevailed over the study area in winter (Fig. 3b and Fig. 3d). Fig. 4 shows the gridded observation and simulated precipitation in summer and winter. Precipitation in summer was much greater than that in winter for both the observation and simulation. WRF-Chem precipitation realistically represented the position of the rain band in summer. The relatively low precipitation values in Xinjiang and high values in southern TP were also well reproduced (Fig. 4a and Fig. 4c). Furthermore, in comparison with the CRU dataset (Fig. 4c and Fig. 4d), the WRF-Chem simulation showed more subtle orographic pattern such as high precipitation along the Tianshan Mountains and the Himalayas. Such a result is due to the fact that the CRU precipitation was interpolated from meteorological stations that were concentrated in the valleys and experienced lower precipitation than mountainous locations, which led to a large underestimation of precipitation in unpopulated mountainous regions (Ji et al., 2015).

To quantitatively evaluate the simulation precision for surface meteorological elements over western China, the meteorological data of the 273 national stations were used. Fig. S3 shows the comparisons between the measured and simulated T2, 2-m relative humidity (RH2), and surface wind speed (U10) with box plots in summer and winter, respectively. The model showed higher T2 in summer (mean bias (MB)

was equal to 2.2 °C), but lower T2 in winter (MB=－1.5 °C). Conversely, the model showed lower RH2 in summer (MB=－6.1 %) and slightly higher RH2 in winter (MB=1.9 %). U10 was not simulated as well as T2 and RH2. The mean of correlation coefficients in summer and winter were equal to 0. 87, 0.73, and 0.51 for T2, RH2 and U10, respectively. The statistics between the observations and simulations are presented in Supplementary Table S1.

3.1.2. BC concentration

Fig. 5 shows surface BC concentrations from the WRF-Chem simulation (Fig. 5a and Fig. 5b) and MOZART (Fig. 5c and Fig. 5d) in summer and winter. Both WRF-Chem and MOZART results indicated that the BC concentration in summer was lower than that in winter. This is because the weather condition in summer was favorable to dilute and diffuse air pollutants, including smallest pressure, largest boundary layer height and largest precipitation (Fig. S4). In summer, BC was concentrated in the Sichuan and Guanzhong basins, which are located to the east of the TP. BC concentrations in Xinjiang province were not as high as in Sichuan province, but higher than those over the TP. In winter, a center of intense BC concentration appeared in the Sichuan Basin, which was caused by the high emission of this region and the meteorological conditions which were not conducive to diffusing air pollution (Che et al., 2009). As shown in Fig. S5, there was a significant seasonal variation of BC from the MEIC emission inventory with higher values in winter (Fig. S5b) compared with in summer (Fig. S5a), due to greater energy demand such as the fossil-fuel and biofuel usage for residential winter heating. The

comparison between WRF-Chem and MOZART showed that WRF-Chem captured the overall spatial and seasonal patterns of BC aerosol concentrations in western China.

We further summarized surface BC concentrations from 12 sites to evaluate the model simulations in western China (Table 2). Our results showed that atmospheric BC concentrations were lower in the remote areas of the TP. At Namco, Lhasa and Qomalangma, surface BC concentrations were less than 0.5 μg m^{-3}. High BC concentrations appeared over the urban sites in highly populated regions (Xi'an, Lanzhou, and Urumqi), at more than 10 times greater than that in the TP. Furthermore, BC concentrations were higher on TP's edge (e.g., Laohugou and Qinghai Lake) than that in the inland TP (e.g., Beiluhe), due to enriched by the proximity to sources. The WRF-Chem model well represented the spatial variation at these sites. In addition, the seasonal variation of BC concentration at Qomalangma was well reproduced by the model (Fig. S6), with *R* equal to 0.74. Both the simulation and observation showed high BC concentrations in the non-monsoon season and low values in the monsoon season.

3.2. Contributions to BC concentrations from different sources

The model performance indicates that this modeling framework is appropriate for quantifying the relative roles of various BC sources. Moreover, in consideration of large differences in simulated BC concentrations between the HM region (5.48 ug m^{-3} in summer, 7.16 ug m^{-3} in winter) and the RB region (0.09 ug m^{-3} in summer, 0.15 ug m^{-3} in winter), we investigated the differences in the contribution of individual

emission sectors to BC concentrations in these two typical regions.

3.2.1. Spatial distribution of BC concentrations from different sources

Fig. 6 presents the spatial distribution of the annual average modeled BC concentrations from total emission and from each individual source. Low concentrations of annual mean total BC concentrations appeared over the TP, northern Gansu province, and most of Xinjiang province, while high concentrations occurred in the Sichuan and Guanzhong basins (Fig. 6a). From Table 3, the annual mean BC concentrations in the RB region was only 0.12 μg m^{-3}, but the corresponding values reached 6.31 μg m^{-3} in the HM region.

Among the sectorial contributions to total BC concentrations, the residential contribution was significantly higher than those of other emission sources (Fig. 7). As shown in Fig. 7a, the residential contribution to the annual mean BC concentration was larger than 50 %, especially in the RB region where it exceeds 70 % (with a mean of 71.2 % listed in Table 2). The larger residential contribution in the RB region was due to local emissions as well as long-distance transport. As shown in supplement Fig. S6, residential sources from South Asia contributed significantly to BC concentrations over the TP. Due to the low level of economic development, industrial and transportation sources only contributed 0.013 μg m^{-3} (11.3 %) and 0.022 μg m^{-3} (17.4 %) to the total BC concentration there.

The residential contribution to the annual mean BC concentration in the HM region was 68.6%. Due to the more developed industry and busy transportation in the HM region, the spatial distribution of BC concentration from industry (1.42 μg m^{-3})

and transportation (0.56 μg m^{-3}) showed higher values than in the TP region, with the contribution ratios of 22.5% and 9% to the total BC concentration. Transportation was the next largest BC source in the RB region. Although the BC concentration from transportation was much lower in the RB region (0.022 μg m^{-3}) than that in the HM region (0.56 μg m^{-3}), its average contribution ratio to the total surface BC concentration was higher in the RB region (17.4%) than that in the HM region (9%). In northern Xinjiang, the industrial source contribution reached 50% to the annual mean BC concentration in some parts (Fig. 7b), which was higher contribution than that in the HM region with highly populated urban mega-cities. The larger relative contribution of industry in northern Xingjiang was because of the relatively smaller influence of residential emissions there compared to residential emissions in the HM region as shown in Fig. 7a. Power generation played a minor role in the annual average BC concentration (Fig. 7d and Fig. 7e), with the mean contribution rate less than 0.1 % in both the RB and HM regions. Compared with very little BC (0.03%) from open biomass burning in the HM region, 2.1% surface BC emission were from open fire in the TP. The results above describing sectorial contributions to annual mean BC concentrations in the HM and RB regions are summarized in Table 3.

Fig. 8 shows the sectorial contributions to modeled annual mean BC at seven typical sites in western China. For the sites in remote areas, the residential contribution rate reached 75.9% and 87.3% at Namco and Qomolangma sites, respectively. Previous studies have found that BC aerosol in the southern TP (such as at Qomolangma) was mainly influenced by long-distance transport from South Asia

(Yang et al., 2017b). Where, residential emission sources were prevalent, including open combustion of garbage and crop residues, brick kilns and household cooking/heating with firewood, and the burning of animal dung and coal briquettes (Li et al., 2016a). Therefore, the residential sector in South Asia was an important source of BC for the TP (Fig. S7). At the urban sites of Xi'an, Lanzhou, Lhasa, and Urumqi, residential emissions contributed 68.7 %, 69.8%, 63.5%, and 46.4%, respectively. The next largest contributor to BC concentration at the urban sites was the industrial source. Our result is consistent with that of a previous modeling study at Xi'an city (Li et al., 2016c), which pointed out that residential emission contributed the most to BC concentrations there, followed by industrial and transportation sources. However, for Lhasa city, the transportation sector's contribution to total BC concentration was 9.8% larger than the industry source. The transportation source showed a larger influence to surface BC concentration at Namco (14.6%) than that at Qomolangma (5.5%), because transportation was more developed at Namco.

3.2.2. Seasonal variation of BC concentrations from different sources and its relationship with meteorological parameters

The WRF-Chem simulation results indicated that total BC concentrations over western China were significantly lower in summer (Fig. 5a) than that in winter (Fig. 5b). As shown in Table 3, the total BC concentration during winter was nearly doubled that of during summer in the RB region. The seasonal variation of total BC concentration in the HM region was relatively smaller, with the value equal to 5.48 μg m^{-3} in summer and 7.1 μg m^{-3} in winter, an increase of 30.7%.

The simulated BC concentrations from each individual sector during summer and winter are presented in Fig. 9 and Fig. 11, respectively, with the corresponding proportions to the total BC concentrations presented in Fig. 10 and Fig. 12. It can be seen that BC concentrations from various emission sectors were all lower in summer (Fig. 9) than that in winter (Fig. 11). For example, for the residential sector, lower BC concentrations appeared in both the RB and HM regions during summer (Fig. 9a), compared with that during winter (Fig. 11a). However, there was remarkable seasonal variation in the relative contribution of different emission sources to the total BC. In the RB region, the industrial and transportation sectors showed a larger relative contribution to the total BC in summer (Fig. 10b and Fig. 10c) compared to in winter (Fig. 12b and Fig. 12c), but the residential sector showed smaller contribution in summer compared to winter (Fig. 10a). Specifically, as shown in Table 3, the largest difference of BC concentrations between summer and winter was from the residential emission source (0.068 μg m^{-3}) in the RB region, followed by the transportation (0.002 μg m^{-3}) and the industrial (0.011μg m^{-3}) sources. In terms of relative contribution to the change of total BC concentrations, these values were 9.0%, -5.8%, and -3.2%. In the HM region, the differences in BC concentration between summer and winter in residential, industry, and transportation sources were 1.14 μg m^{-3}, 0.44 μg m^{-3}, and 0.21 μg m^{-3}. Although considerably larger in absolute value than concentration change in the RB region, the corresponding changes in relative contributions to total BC concentrations were less than 1.0% (-0.3 %, 0.9 %, and 0.8 % for residential, industrial, and transportation sources, respectively). We also calculated

proportional contribution of each individual sector to the total BC concentrations in spring (Fig. S8) and autumn (Fig. S9) seasons. Over the TP in both seasons, the residential sector remained the largest contributor to BC concentrations and the transportation sector also displayed higher influence in BC than the industrial sector.

Finally, we calculated the contributions of various sectors to the seasonal variation (from summer to winter) of total BC, where a sector's contribution is equal to the proportion of that sector's BC change in the total BC change. The results showed that the residential, industrial, transportation sectors explain 84.0%, 2.5%, and 13.6% of BC seasonal variation in the RB region, and 63.6 %, 24.6 %, and 11.7 % of BC seasonal variation in the HM region (Fig. S10). It indicated that the seasonal variation of the total BC concentration was mainly affected by the residential emission sector. The industrial sector contributed much more to the BC seasonal variation in the HM region (24.6%) than that in the RB region (2.5%). Compared with the residential and industrial emission sources, the influence of transportation sector was relatively low (11.7 %) in the HM region. However, the contribution from the transportation sector (13.6%) to BC seasonal variation in the RB region was much larger than the industrial sector (2.5%).

In summary, the residential sector was an impact factor causing increased BC concentrations in winter in western China, such as the fossil-fuel and biofuel usage for residential winter heating. Further, we analyze the impact of meteorological conditions on BC concentrations seasonal variation. Fig. 13 compares the daily variation of simulated BC concentrations with various meteorological factors

averaged in western China. The results indicated that the high BC concentrations in winter showed a consistency with lower boundary layer height, relatively weaker winds, less precipitation and lower temperature, which can further exacerbate air pollution due to less precipitation wet scavenging, and poor diffusion and diluted conditions.

3.3 Evaluation of emission control strategies to reduce BC pollution

In the above section, we evaluated the contribution of individual sectors to surface BC concentrations in western China, and further compared the differences between the HM and the RB regions. Here, we will assess the emission control strategies to reduce BC pollution by analyzing three sensitivity experiments, where residential, industry, transportation BC emission sources were reduced by 50% successively. As shown in Fig. 14, a 50% reduction of the residential emissions caused 36.2% and 36.7% respective decreases in the annual mean surface BC concentration of the RB or HM regions. The decrease ratios of surface BC concentration reached the largest in winter (37.1% in the RB region and 38.6% in the HM region). However, a 50% reduction of industrial or transportation emissions only caused less than 12% decrease in the annual mean surface BC concentration of the RB or HM regions. This result again indicated that the residential sector was the largest emission source in western China. Similar to other highly industrialized regions (e.g. in Northern China; Li et al., 2017b), a 50% reduction of industrial emission caused the second largest decrease (10.9%) of BC concentration in the HM region. However, a 50% reduction of transportation emissions led to a 9.2% decrease in BC

concentration in the RB region, larger than the 5.9% decrease caused by a 50% reduction of the industrial emissions. Therefore, unlike in the HM region with highly populated mega-cities, policy makers should pay more attention to transportation emissions when designing control strategies for BC pollution in the RB region over the TP.

4. Conclusion

In this first source apportionment and emission control assessment study for western China including the TP using the WRF-Chem model, we used the WRF-Chem version 3.6.1 to simulate surface black carbon (BC) concentrations over western China from June 2016 to May 2017, in order to quantify the contribution of individual emission sources to BC concentrations in that region. First, we evaluated WRF-Chem's performance in simulating meteorological elements and surface BC concentrations, by comparing simulations against gridded and in situ observations. Then, we quantitatively assessed the spatial and temporal characteristics of BC concentrations from each individual source, and compared the sectoral contributions to the simulated BC concentrations between the urban (HM) and background (RB) regions.

It was found that the WRF-Chem model captured the main spatial and temporal features of meteorological elements and surface BC concentrations in western China, adding confidence to the apportionment of the sources of BC. Simulated results clearly indicated that the residential sector was the largest contributor to the annual BC concentrations in western China. The next largest BC sources for the HM (mean

contribution ratio of 22.5 %) and the RB region (mean contribution ratio of 17.4 %) were the industrial sector and the transportation sector respectively. Emissions from power plants (less than 0.1%) and open biomass burning sources (less than 1%) played minor roles in the total BC concentration. Clear seasonality in the BC concentration of the study region was observed, with total BC concentrations lower in summer than in winter. In terms of relative contribution, the seasonal variation of BC contributions was greater in the RB region than in the HM region, mainly affected by residential emissions which explain 84 % and 63.6 % of the BC concentration change in the RB and HM regions, respectively. Additionally, lower boundary layer height, weaker winds, less precipitation and lower temperature in winter can further exacerbate air pollution due to less precipitation wet scavenging, as well as poor diffusion and diluted conditions.

An evaluation of emission control strategies suggested that a 50% reduction of the residential emissions resulted in a 36.2% or 36.7% decrease in the annual mean surface BC concentrations in the RB or HM region, respectively. The decrease ratio of BC concentration was highest in winter, being 37.1% in the RB region and 38.6% in the HM region. A 50% reduction in industry or transportation emissions only led to less than 12% decreases in the BC concentrations in either the RB or HM region. Unlike in highly industrialized region, a 50% reduction of the transportation emissions led to a 9.2% decrease in the BC concentration in the RB region, larger than that caused by a 50% reduction of the industrial emissions. More attention should be paid to transportation emissions when designing control strategies for air pollution

over the TP. The results from this work provide useful information for local governments to prepare and implement air pollution guidelines in western China.

Acknowledgments

This study was supported by the National Natural Science Foundation of China (41603129, 41701074, 91644225) and the Key Research Program of the Chinese Academy of Sciences (QYZDJ-SSW-DOC039), the Open Program (SKLCS-OP-2017-02, SKLCS-OP-2018-09) from State Key Laboratory of Cryospheric Science, Northwest Institute of Eco-Environment and Resources, Chinese Academy of Sciences, and the China Postdoctoral Science Foundation (2016M602896). Deliang Chen was supported by the Strategic Priority Research Program of Chinese Academy of Sciences (XDA20060401), as well as the Swedish VR, STINT, and Merge.

Reference

Anenberg, S.C., Schwartz, J., Shindell, D., Amann, M., Faluvegi, G., Klimont, Z., Janssens-Maenhout, G., Pozzoli. L., van-Dingenen, R., vignati, E., et al., 2012. Global air quality and health co-benefits of mitigating near-term climate change through methane and black carbon emission controls. Environ. Health. Persp. 120, 831−839.

Bond, T.C., Doherty, S.J., Fahey, D.W., Forster, P.M., Berntsen, T., DeAngelo, B.J., Flanner, M.G., Ghan, S., Kärcher, B., Koch, D., Kinne, S., Kondo, Y., Quinn, P.K., Sarofim, M.C., Schultz, M.G., Schulz, M., Venkataraman, C., Zhang, H., Zhang, S., Bellouin, N., Guttikunda, S.K., Hopke, P.K., Jacobson, M.Z., Kaiser, J.W., Klimont, Z., Lohmann, U., Schwarz, J.P., Shindell, D., Storelvmo, T., Warren, S.G., Zender, C.S., 2013. Bounding the role of black carbon in the climate system: A scientific assessment. J. Geophys. Res.-Atmos., 118, 5380–5552.

Boucher, O., Randall, D., Artaxo, P., Bretherton, C., Feingold, G., Forster, P., Kerminen, V.M., Kondo, Y., Liao, H., Lohmann, U., et al., 2013. Clouds and Aerosols. In Climate Change 2013: The Physical Science Basis. Contribution of Working Group I to the Fifth Assessment Report of the Intergovernmental Panel on Climate Change. Stocker, T. F., et al. Eds.; Cambridge Univ. Press: Cambridge and New York.

Cao, J.J, Xu, B.Q., He, J.Q., Liu, X., Han, Y., Wang, G., Zhu, C., 2009. Concentrations, seasonal variations, and transport of carbonaceous aerosols at a

remote Mountainous region in western China. Atmos. Environ., 43, 4444–4452.

Cao, J.J., Wang, Q.Y., Chow, J.C., Watson, J.G., Tie, X.X., Shen, Z.X., Wang, P., An, Z.S., 2012. Impacts of aerosol compositions on visibility impairment in Xi'an, China. Atmos. Environ. 59, 559–566.

Che, H.Z., Zhang, X.Y., Li, Y., Zhou, Z.J., Qu, J.J., Hao, X.J., 2009. Haze trends over the capital cities of 31 provinces in China, 1981–2005. Theor. Appl. Climatol. 97, 235–242.

Chen, D., Xu, B., Yao, T., Guo, Z., Cui, P., Chen, F., Zhang, R., Zhang, X., Zhang, Y., Fan, J., Hou, Z., Zhang T., 2015. Assessment of past, present and future environmental changes on the Tibetan Plateau. Chinese Science Bulletin, 60, 3025–3035 (in Chinese).

Chen, F., Dudhia, J., 2001. Coupling an advanced land surface-hydrology model with the Penn State-NCAR MM5 modeling system. Part I: Model implementation and sensitivity. Mon. Weather. Rev. 129, 569–585.

Dachs, J., Eisenreich, S.J., 2000. Adsorption onto aerosol soot carbon dominates gasparticle partitioning of polycyclic aromatic hydrocarbons. Environ. Sci. Technol. 34, 3690–3697.

Dee, D.P., Uppala, S.M., Simmons, A.J., et al., 2011. The ERA-interim reanalysis: configuration and performance of the data assimilation system. Q. J. R. Meteorol. Soc. 137, 553–597.

Emmons, L.K., Walters, S., Hess, P.G., Lamarque, J.F., Pfister, G.G., Fillmore, D., Granier, C., Guenther, A., Kinnison, D., Laepple, T., Orlando, J., Tie, X., Tyndall,

G., Wiedinmyer, C., Baughcum, S.L., Kloster, S., 2010. Description and evaluation of the Model for Ozone and Related chemical Tracers, version 4 (MOZART-4). Geosci. Model. Dev. 3, 43–67.

Flanner, M.G., Zender, C.S., Randerson, J.T., Rasch, P.J., 2007. Present day climate forcing and response from black carbon in snow. J. Geophys. Res.-Atmos. 112, 1013–1029.

Freitas, S.R., Longo, K.M., Alonso, M.F., Pirre, M., Marecal, V., Grell, G., Stockler, R., Mello, R. F., Sánchez, G. M., 2011. PREP-CHEM-SRC–1.0: a reprocessor of trace gas and aerosol emission fields for regional and global atmospheric chemistry models. Geosci. Model. Dev. 4, 419–433.

Gao, Y., Zhang, M., Liu, Z., Wang, L., Wang, P., Xia, X., Tao, M., Zhu, L., 2015. Modeling the feedback between aerosol and meteorological variables in the atmospheric boundary layer during a severe fog–haze event over the North China Plain. Atmos. Chem. Phys. 15, 4279–4295.

Grell, G.A., Peckham, S.E., Schmitzc, R., McKeenb, S.A., Frostb, G., Skamarockd, W.C., Eder, B., 2005. Fully coupled ‘‘online’’ chemistry within the WRF model. Atmos. Environ. 39, 6957–6975.

Hansen, J., Nazarenko, L., 2004. Soot climate forcing via snow and ice albedos. P. Natl. Acad. Sci. USA. 101, 423–428.

Ji, Z.M., Kang, S.C., Cong, Z.Y., Zhang, Q.G., Yao, T.D., 2015. Simulation of carbonaceous aerosols over the Third Pole and adjacent regions: distribution, transportation, deposition, and climatic effects. Clim. Dyn. 45, 2831–2846.

Ji, Z.M., 2016a. Modeling black carbon and its potential radiative effects over the Tibetan Plateau. Advances in Climate Change Research. 7, 139–144.

Ji, Z.M,, Kang SC, Zhang QG, Cong ZY, Chen PF, Sillanpää M. 2016b. Investigation of mineral aerosols radiative effects over High Mountain Asia in 1990–2009 using a regional climate model. Atmos. Res. 178-179, 484–496

Kang, S.C., Cong, Z.Y., 2016. Atmospheric black carbon and its effects on cryosphere. Advances in Climate Change Research. 7, 113–114.

Lau, K.M., Kim, M.K., Kim, K.M., 2006. Asian monsoon anomalies induced by aerosol direct effects. Clim. Dyn. 26, 855–864.

Lei, Y., Zhang, Q., He, K.B., et al., 2011. Primary anthropogenic aerosol emission trends for China, 1990–2005. Atmos. Chem. Phys. 2011, 17153–17212.

Li, Y.J., Zhang, L., Cao, X.J., Yun, Y., Shi, J.S., 2014. Property of black carbon concentration over urban and suburban of Lanzhou. J. Environ. Sci.-China. 34, 1397–1403.

Li, C.L., Bosch, C., Kang, S.C., et al., 2016a. Sources of black carbon to the Himalayan–Tibetan Plateau glaciers. Nat. Commun. 2016a, 7, 12574.

Li, C.L., Yan, F.P., Kang, S.C., Chen, P.F., Hu, Z.F., et al., 2016c. Light absorption characteristics of carbonaceous aerosols in two remote stations of the southern fringe of the Tibetan Plateau, China. Atmos. Environ. 143, 79–85.

Li, M., Zhang, Q., Kurokawa, J., Woo, J.H., He, K.B., Lu, Z., Ohara, T., Song, Y., Streets, D.G., Carmichael, G.R., Cheng, Y.F., Hong, C.P., Huo, H., Jiang, X.J., Kang, S.C., Liu, F., Su, H., Zheng, B., 2017b. MIX: a mosaic Asian

anthropogenic emission inventory for the MICS-Asia and the HTAP projects. Atmos. Chem. Phys. 17, 935-963.

Li, N., He, Q., Tie, X., Cao, J.J., Liu, S.X., Wang, Q.W., Li, G.H., Huang, R.J., Zhang, Q., 2016b. Quantifying sources of elemental carbon over the Guanzhong Basin of China: A consistent network of measurements and WRF-Chem modeling. Environ. Pollut. 214, 86–93.

Li, X.F., Kang, S.C., Zhang, G.S., Qu, B., Tripathee, L., Paudyal, R., Jing, Z.F., Zhang, Y.L., Yan, F.P., Li, Y., Cui, X.Q., Xu, R., Hu, Z.F., Li, C.L., Light-absorbing impurities in a southern tibetan plateau glacier: variations and potential impact on snow albedo and radiative forcing. Atmos. Res. 200, 77–87.

Liu, X.C., Zhong, Y.T., He, Q., Yang, X.H., Ali, M., 2013. Change character of black carbon concentration in atmosphere in Urumqi and the effect factors. Desert and Qasis Meteorology, 7, 36–42 (in Chinese).

Lu, Z., Zhang, Q., Streets, D.G., 2011. Sulfur dioxide and primary carbonaceous aerosol emissions in China and India, 1996–2010. Atmos. Chem. Phys. 11, 9839–9864.

Mitchell, T.D., Jones, P.D., 2005. An improved method of constructing a database of monthly climate observations and associated high resolution grids. Int. J. Climatol. 25, 693–712.

Morrison, H., Thompson, G., Tatarskii, V., 2009. Impact of Cloud Microphysics on the Development of Trailing Stratiform Precipitation in a Simulated Squall Line: Comparison of One- and Two-Moment Schemes. Mon. Weather Rev. 137, 991–

1007.

Niu, H.W., Kang, S.C., Wang, H.L., Zhang, R.D., Lu, X.X., Qian, Y., Paudyal, R., Wang, S.J., Shi, X.F., Yan, X.G., 2018. Seasonal variation and light absorption property of carbonaceous aerosol in a typical glacier region of the southeastern Tibetan Plateau. Atmos. Chem. Phys. 18, 6441–6460.

Ramanathan, V., Ramana, M.V., Roberts, G., Kim, D., Corrigan, C., Chung, C., Winker, D., 2007. Warming trends in Asia amplified by brown clouds solar absorption. Nature. 448, 575–578.

Schaefer, J.T., 1990. The critical success index as an indicator of warning skill.Weather. Forecast. 5, 570–575.

Skamarock, W.C., Klemp, J.B., Dudhia, J., Gill, D.O., Barker, D.M., Wang, W., Powers, J.D., 2005. A description of the Advanced Research WRF version 2, Tech Rep TN-468+STR, p 8, Natl Cent Atmos Res Boulder Colo.

Streets, D.G, Bond, T.C., Carmichael, G.R, et al., 2003. An inventory of gaseous and primary aerosol emissions in Asia in the year 2000. J. Geophys. Res.-Atmos. 108, GTE 30-1.

Wang, K., Zhang, Y., Yahya, K., Wu, S.Y., Georg, G., 2014. Implementation and initial application of new chemistry-aerosol options in WRF/Chem for simulating secondary organic aerosols and aerosol indirect effects for regional air quality. Atmos. Environ., 115, 716–732.

Wang, M., Xu, B.Q., Wang, N.L., Cao, J.J., Tie, X.X., Wang, H.L., et al., 2016. Two distinct patterns of seasonal variation of airborne black carbon over Tibetan

Plateau. Sci. Total. Environ. 573, 1041–1052.

Wiedinmyer, C., Akagi, S.K., Yokelson, R.J., Emmons, L.K., 2010. The Fire INventory from NCAR (FINN): a high resolution global model to estimate the emissions from open burning, Geosci. Model. Dev. Discuss., 3, 625–641.

Xu, B., Cao, J., Joswiak, D.R., Liu, X., Zhao, H., He, J., 2012. Post-depositional enrichment of black soot in snow-pack and accelerated melting of Tibetan glaciers. Environ. Res. Lett. 7, 014022.

Yang, J.H., Duan, K.Q., Kang, S.C., Shi, P.H., Ji, Z.M., 2017a. Potential feedback between aerosols and meteorological conditions in a heavy pollution event over the Tibetan Plateau and Indo-Gangetic Plain. Clim. Dyn. 48, 2901–2917.

Yang, J.H., Kang, S.C., Ji, Z.M., Chen, D.L., 2018. Modeling the origin of anthropogenic black carbon and its climatic effect over the Tibetan Plateau and surrounding regions. J. Geophys. Res.-Atmos. 123, 671–692.

Yang, J.H., Kang, S.C., Ji, Z.M., 2017b. Sensitivity Analysis of Chemical Mechanisms in the WRF-Chem Model in Reconstructing Aerosol Concentrations and Optical Properties in the Tibetan Plateau. Aerosol. Air. Qual. Res. doi: 10.4209/aaqr.2017.05.0156.

Zaveri, R.A., Peters, L.K., 1999. A new lumped structure photochemical mechanism for large-scale applications. J. Geophys. Res.-Atmos. 104, 30387–30415.

Zaveri, R.A., Easter, R.C., Fast, J.D. Peters, L.K., 2008. Model for simulating aerosol interactions and chemistry (MOSAIC). J. Geophys. Res.-Atmos. 113, 1395–1400.

Zhang, Q., Streets, D.G., Carmichael, G.R., He, K., 2009. Asian emissions in 2006 for the NASA INTEX-B missioM. Atmos. Chem. Phys. 9, 5131–5153.

Zhao, C., Liu, X., Ruby, L.L., Hagos, S., 2011. Radiative impact of mineral dust on monsoon precipitation variability over West Africa. Atmos. Chem. Phys. 11. 91–103.

Zhao, S.Y., Ming, J., Xiao, C.D., Sun, W.J., Qin, X., 2012. A preliminary study on measurements of black carbon in the atmosphere of northwest Qilian Shan. J. Environ. Sci. 24, 152–159.

Zhao, Z., Cao, J., Shen, Z., Huang, R.J., Hu, T., Wang, P., et al., 2015. Chemical composition of PM2.5 at a high-altitude regional background site over Northeast of Tibet Plateau. Atmos. Pollut. Res. 6, 815–823.

Zheng, J., He, M., Shen, X., Yin, S., Yuan, Z., 2012. High resolution of black carbon and organic carbon emissions in the Pearl River Delta region, China. Sci. Total Environ. 438, 189–200.

Zhang, Y.L., Kang, S.C., Cong, Z.Y., Schmale, J., Sprenger, M., Li, C.L., Yang, W., Gao, T.G., Sillanpää, M., Li, X.F., Liu, Y.J., Chen, P.F., Zhang, X.L., 2017. Light-absorbing impurities enhance glacier albedo reduction in the southeastern Tibetan plateau. J. Geophys. Res.-Atmos. 122, 6915–6933.

Fig. 1 WRF-Chem modeling domains, topographic field (m) and regional divisions.

Fig. 2 Mean T2 (°C) in summer (a, c) and winter (b, d) from the WRF-Chem simulation (a, b) and the ERA-Interim (c, d) respectively.

Fig. 3 Mean wind speed at 500 hPa (m s^{-1}) in summer (a,c) and winter (b,d) from the WRF-Chem simulation (a,b) and the ERA-Interim (c,d) respectively.

Fig. 4 Cumulative precipitation (mm) in summer (a,c) and winter (b,d) from the WRF-Chem simulation (a,b) and the CRU (c,d) respectively.

Fig. 5 Surface BC concentration (μg m^{-3}) in summer (a,c) and winter (b,d) from the WRF-Chem simulation (a,b) and the MOZART results (c,d) respectively.

Fig. 6 Annual mean simulated BC concentration (μg m^{-3}) from total source and each individual source: (a) total source, (b) residential, (c) industry, (d) transportation, (e) power, and (f) open fire.

Fig. 7 Contribution ratios (%) from each individual source to the annual mean simulated BC concentrations: (a) residential, (b) industry, (c) transportation, (d) power, and (e) open fire.

Fig. 8 Source contributions to the annual mean modeled BC concentration at seven sites in western China. Pie charts present the relative contributions of residential source (blue), industry (red), transportation (green), power (purple), and open biomass burning (orange).

Fig.9 Average summer BC concentration (μg m^{-3}) from total source and each individual source: (a) residential, (b) industry, (c) transportation, (d) power, and (e)

open fire.

Fig. 10 Contribution ratios (%) from each individual source to the summer mean simulated BC concentrations: (a) residential, (b) industry, (c) transportation, (d) power, and (e) open fire.

Fig. 11 Average winter BC concentration (μg m^{-3}) from total source and each individual source: (a) residential, (b) industry, (c) transportation, (d) power, and (e) open fire.

Fig. 12 Contribution ratios (%) from each individual source to the winter mean simulated BC concentrations: (a) residential, (b) industry, (c) transportation, (d) power, and (e) open fire.

Fig. 13 Variations of simulated BC concentrations, boundary layer height (PBLH), surface wind speed (V), precipitation and 2-m temperature (T2) averaged in western China form June 2016 to May 2017.

Fig. 14 Decreased ratios of surface BC concentration in RB (a) and HM (b) regions after a 50% reduction of various anthropogenic sources.

Table 1 Experimental design.

Experiment name	Emissions
Baseline	No emissions are turned off.
S1	Residential emission sector is turned off.
S2	Industry emission sector is turned off.
S3	Transport emission sector is turned off.
S4	Power plant emission sector is turned off.
S5	Open fire emission sector is turned off

Table 2 Observed and simulated surface BC concentration (μg m^{-3}).

Name	Location	m.a.s.l (m)	Time (LT)	Observation	Simulation	
Xi'an	34.23°N 108.9°E	350	2013.5-2014.4	8.7	11.8	*Li et al*. (2016c)
Lanzhou	36.03°N 103.5°E	1520	2010.9-2011.8	7.58	4.51	*Li et al.*(2014)
Wulumuqi	43.82°N 87.62°E	1074	2009.11-2010.2	6.15	1.94	*Liu et al*.(2013)
Lhasa	29.65°N, 91.03°E	3640	2013,3-12	0.46	0.19	*Li et al*. (2015)
Namco	30.77°N 90.98°E	4730	2012,1-12	0.19	0.10	*Wan et al*. (2015)
Beiluhe	34.85°N 92.94°E	4600	2013,1-6	0.49	0.26	Wang et al.(2016)
Qinghai Lake	36.97°N 99.90°E	3300	2012,1-12	0.84	0.58	Zhao et al.(2015)
Laohugou	39.50°N 96.51°E	4214	2009,5-2011,3	0.48	0.24	Zhao et al.(2010)

Tienshan	43.10°N 86.82°E	4130	2004,7-2005,7	0.4	0.17	Xu et al.(2012)
Muztagh Ata	38.29°N 75.02°E	4500	2003,12-2006,12	0.06	0.11	Cao et al.(2009)
Qomalangma	28.36°N 86.95°E	4276	2016,6-2017,5	0.28	0.18	Niu et al.(2018)
Yulong	27.1°N 100.25°E	3054	2016.6-2016,12	1.54	1.01	

	RB			HM		
	Summer	Winter	Annual	Summer	Winter	Annual
Residential	0.055(65.4 %)	0.123(74.4 %)	0.09(71.2%)	3.78(68.9%)	4.92(68.6%)	4.34(68.6%)

Table 3 Mean simulated surface BC concentrations (ug m^{-3}) from different emission sources and relative contribution (%) to the total BC concentrations in RB and HM regions, respectively.

Industry	0.013(14.9%)	0.015(9.1%)	0.015(11.3%)	1.21(22.1%)	1.65(23%)	1.42(22.5%)
Transportation	0.016(19.6%)	0.027(16.4%)	0.022(17.4%)	0.48(8.8%)	0.69(9.6%)	0.56(9.0%)
Total	0.084	0.165	0.129	5.48	7.17	6.31

*Power plant and open fire contribute very little to the regional mean BC concentrations. Thus their contributions are not presented here.

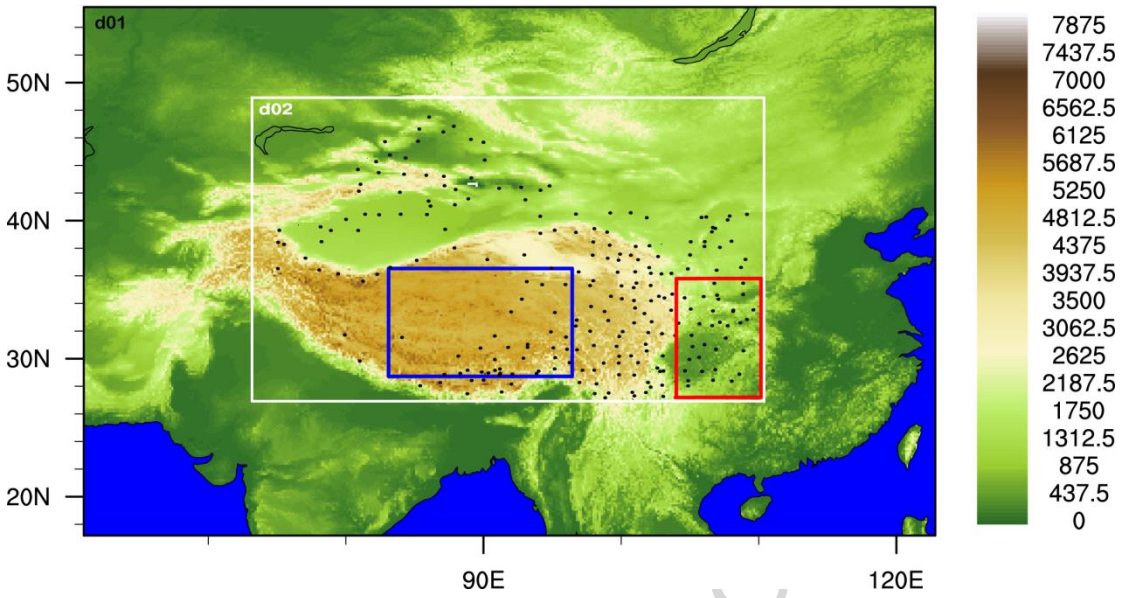

Fig. 1 WRF-Chem modeling domains, topographic field (m) and regional divisions. The national weather stations from the CMDN were noted by black dots. The blue box represented the remote background region RB includes the inner of the TP, and the red box denoted the high population and mega-cities region HM includes eastern Sichuan, Chongqing and southern Shaanxi.

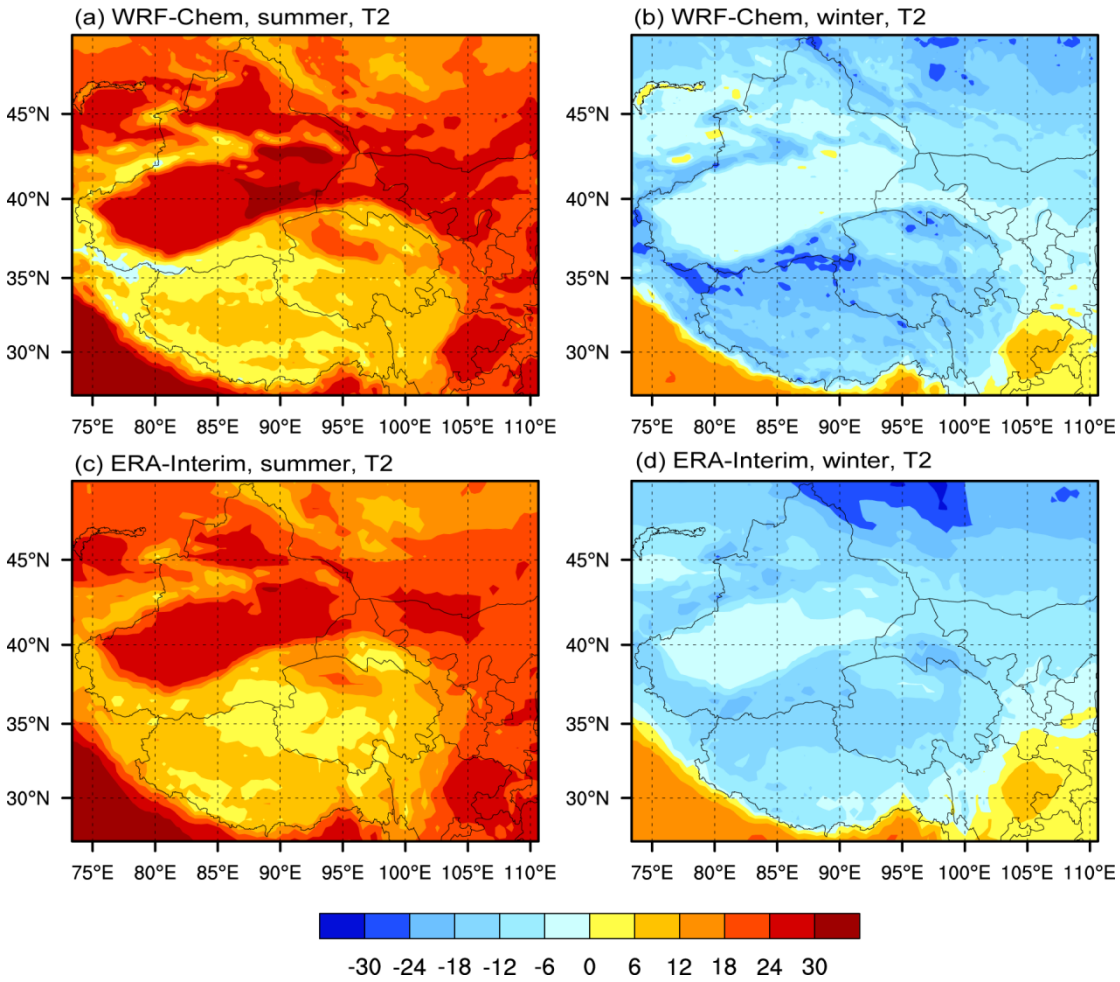

Fig. 2 Mean T2 (°C) in summer (a, c) and winter (b, d) from the WRF-Chem simulation (a, b) and the ERA-Interim (c, d) respectively.

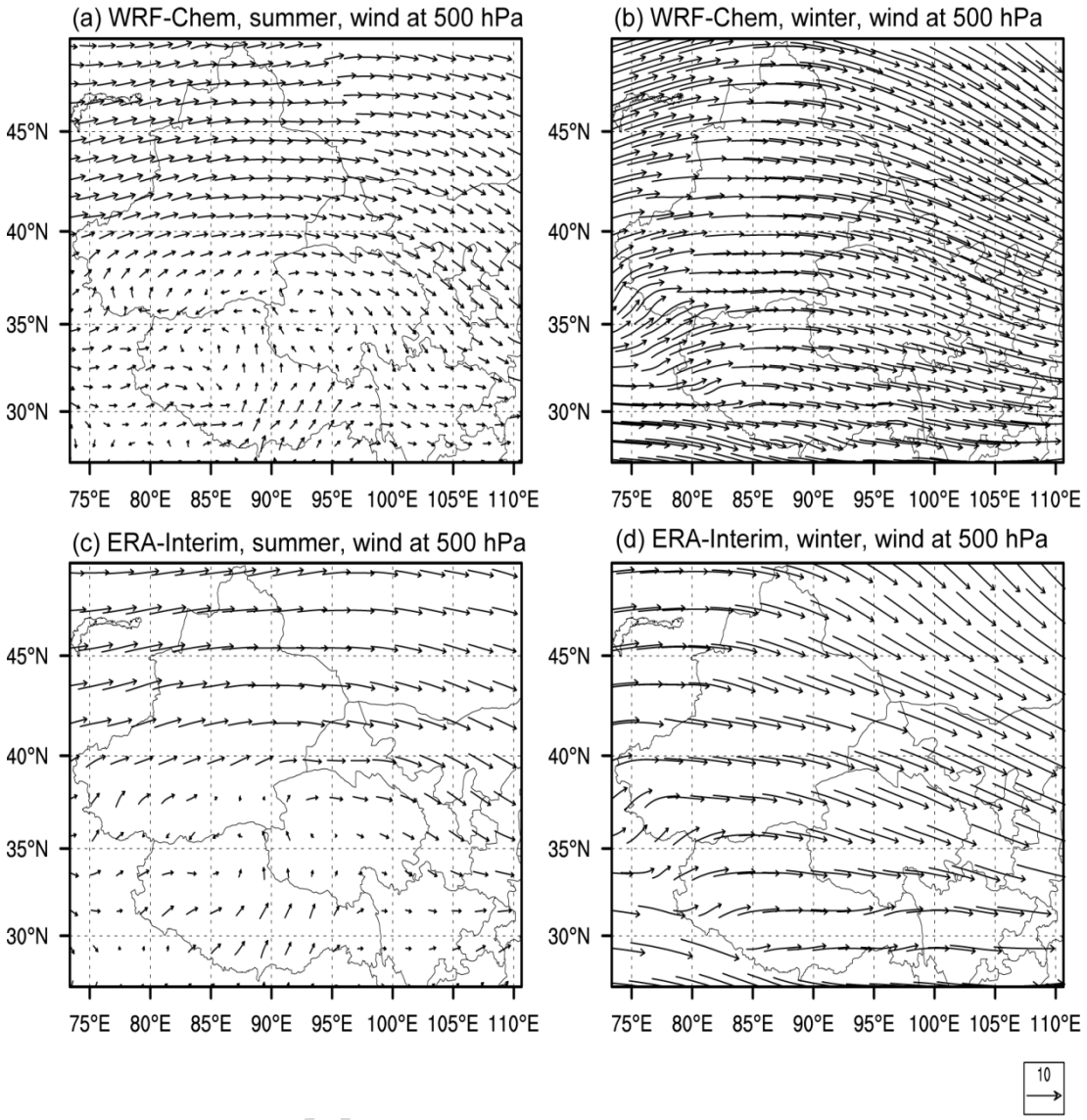

Fig. 3 Mean wind speed at 500 hPa (m s^{-1}) in summer (a,c) and winter (b,d) from the WRF-Chem simulation (a,b) and the ERA-Interim (c,d) respectively.

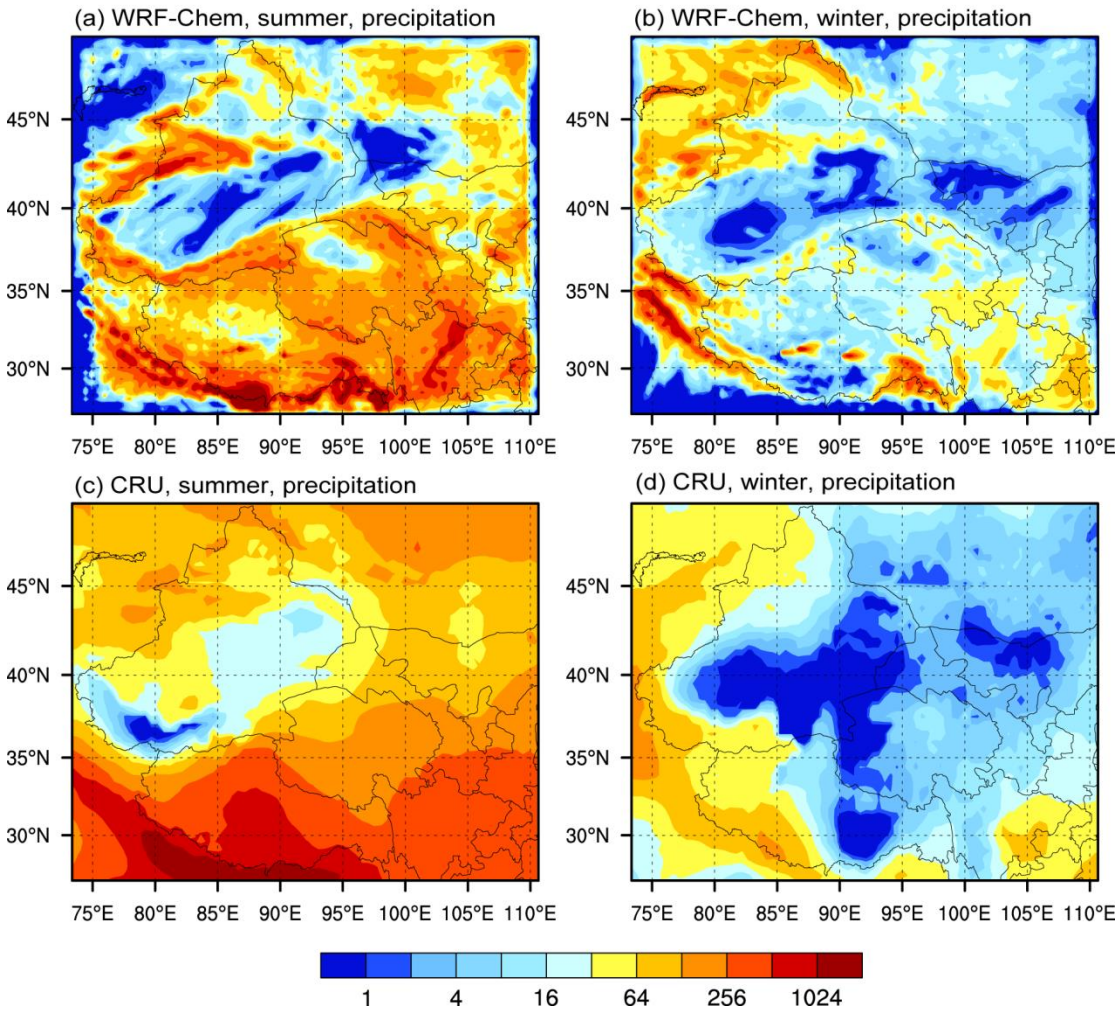

Fig. 4 Cumulative precipitation (mm) in summer (a,c) and winter (b,d) from the WRF-Chem simulation (a,b) and the CRU (c,d) respectively.

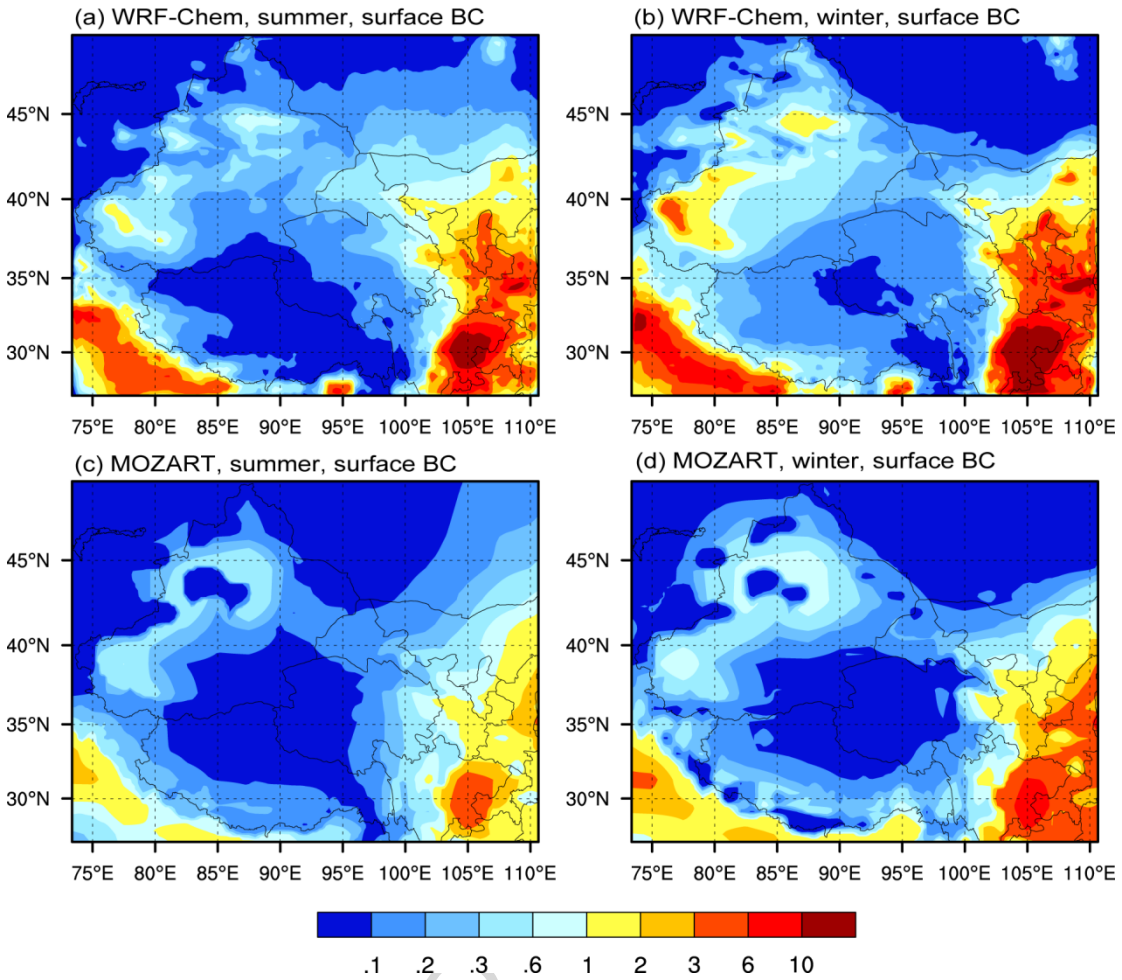

Fig. 5 Surface BC concentration (μg m^{-3}) in summer (a,c) and winter (b,d) from the WRF-Chem simulation (a,b) and the MOZART results (c,d) respectively.

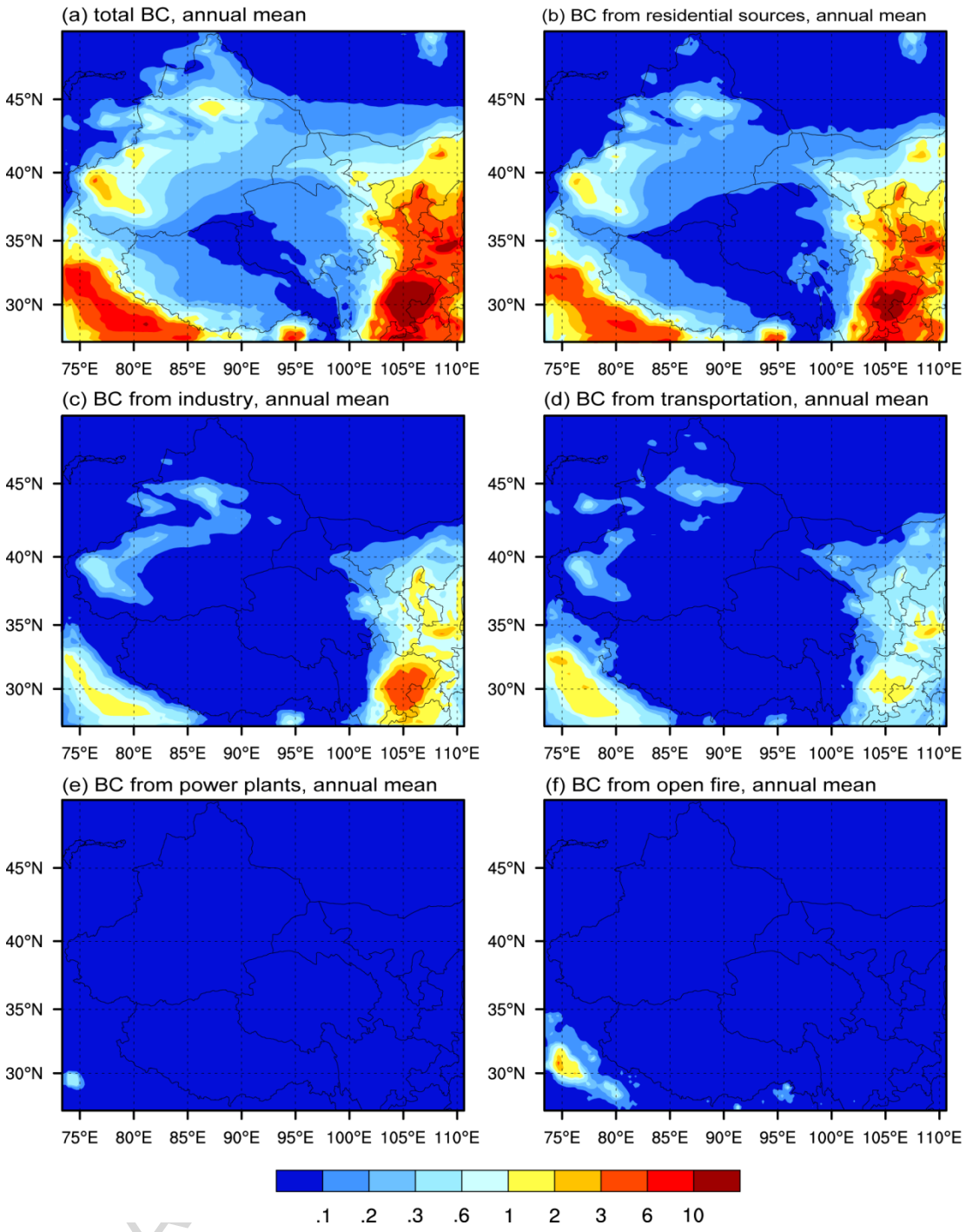

Fig. 6 Annual mean simulated BC concentration (μg m^{-3}) from total source and each individual source: (a) total source, (b) residential, (c) industry, (d) transportation, (e) power, and (f) open fire.

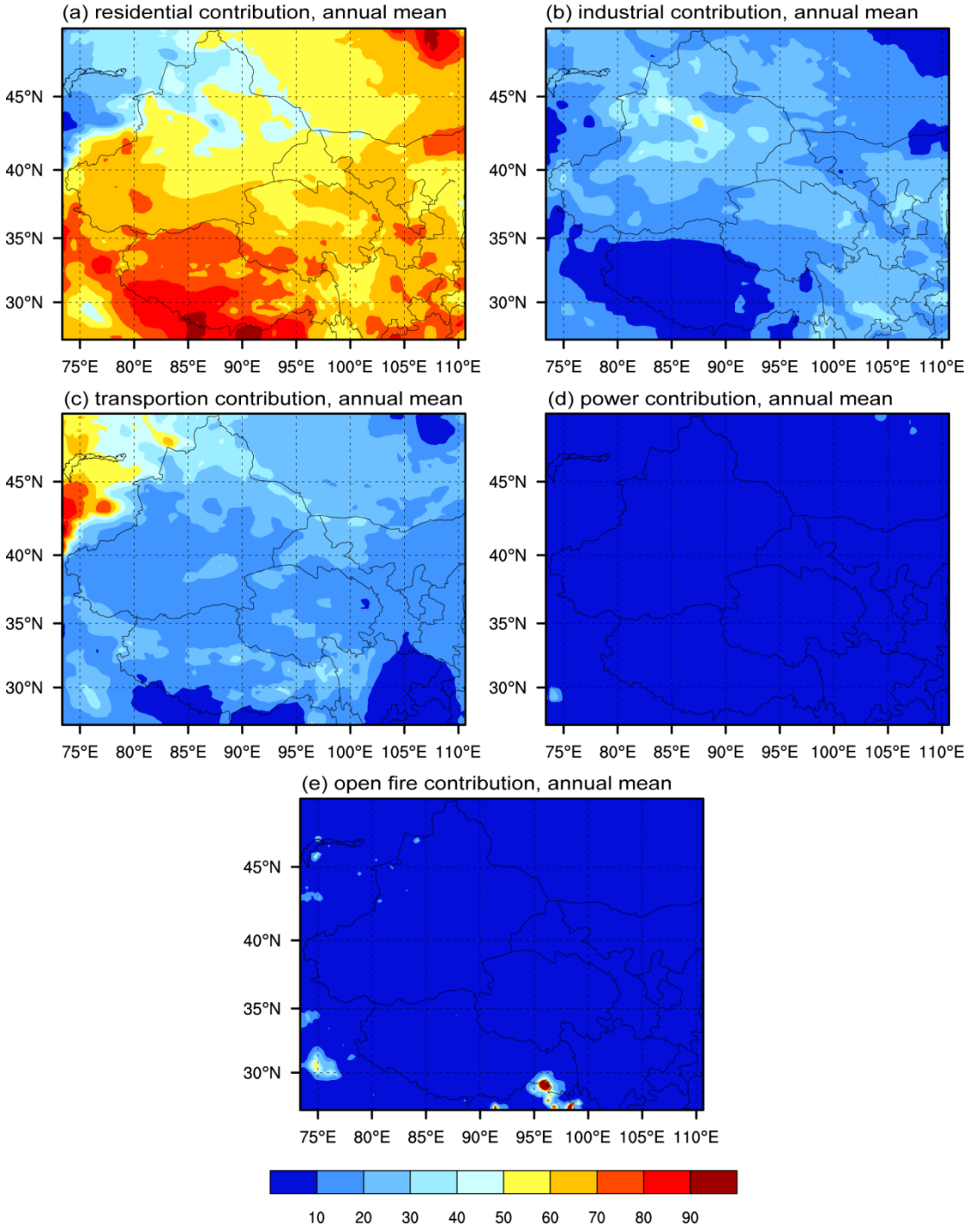

Fig. 7 Contribution ratios (%) from each individual source to the annual mean simulated BC concentrations: (a) residential, (b) industry, (c) transportation, (d) power, and (e) open fire.

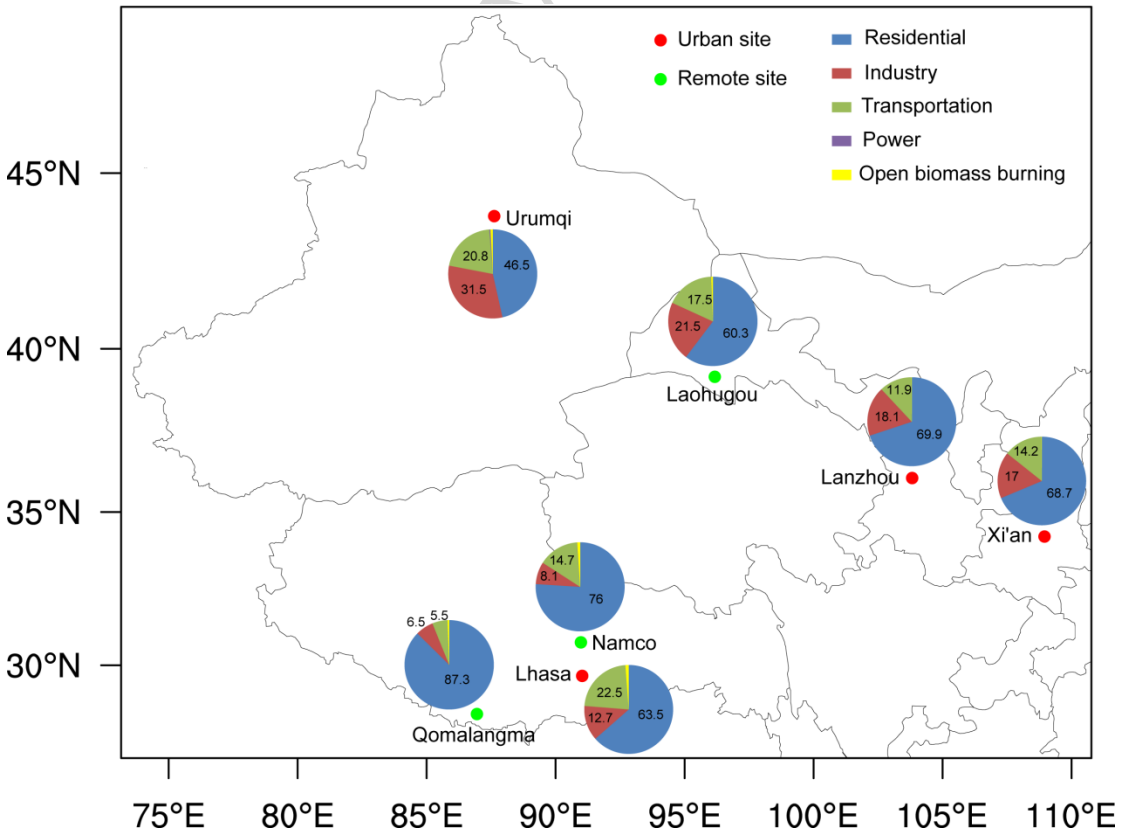

Fig. 8 Source contributions to the annual mean modeled BC concentration at seven

sites in western China. Pie charts present the relative contributions of residential source (blue), industry (red), transportation (green), power (purple), and open biomass burning (orange).

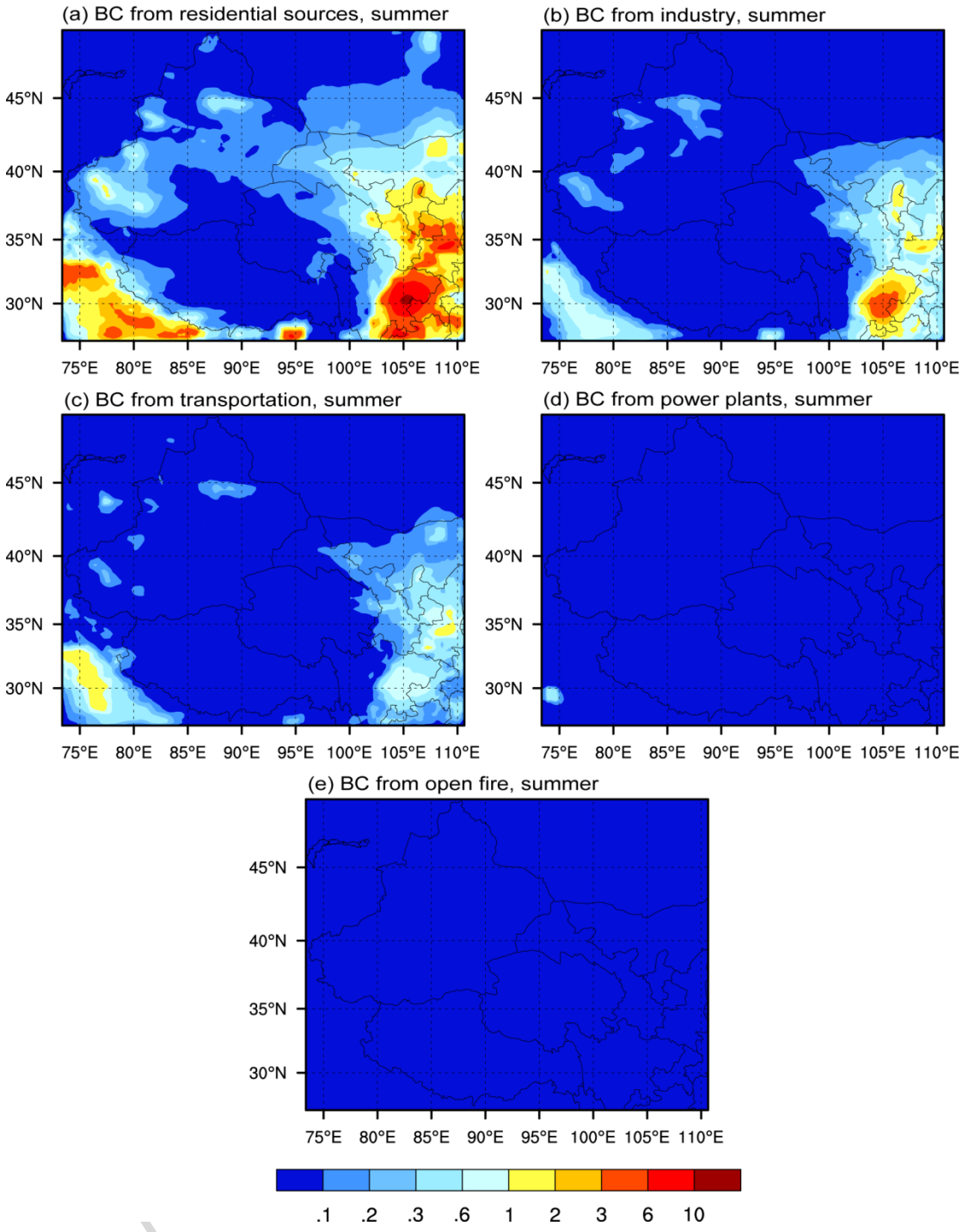

Fig. 9 Average summer BC concentration (μg m^{-3}) from total source and each individual source: (a) residential, (b) industry, (c) transportation, (d) power, and (e) open fire.

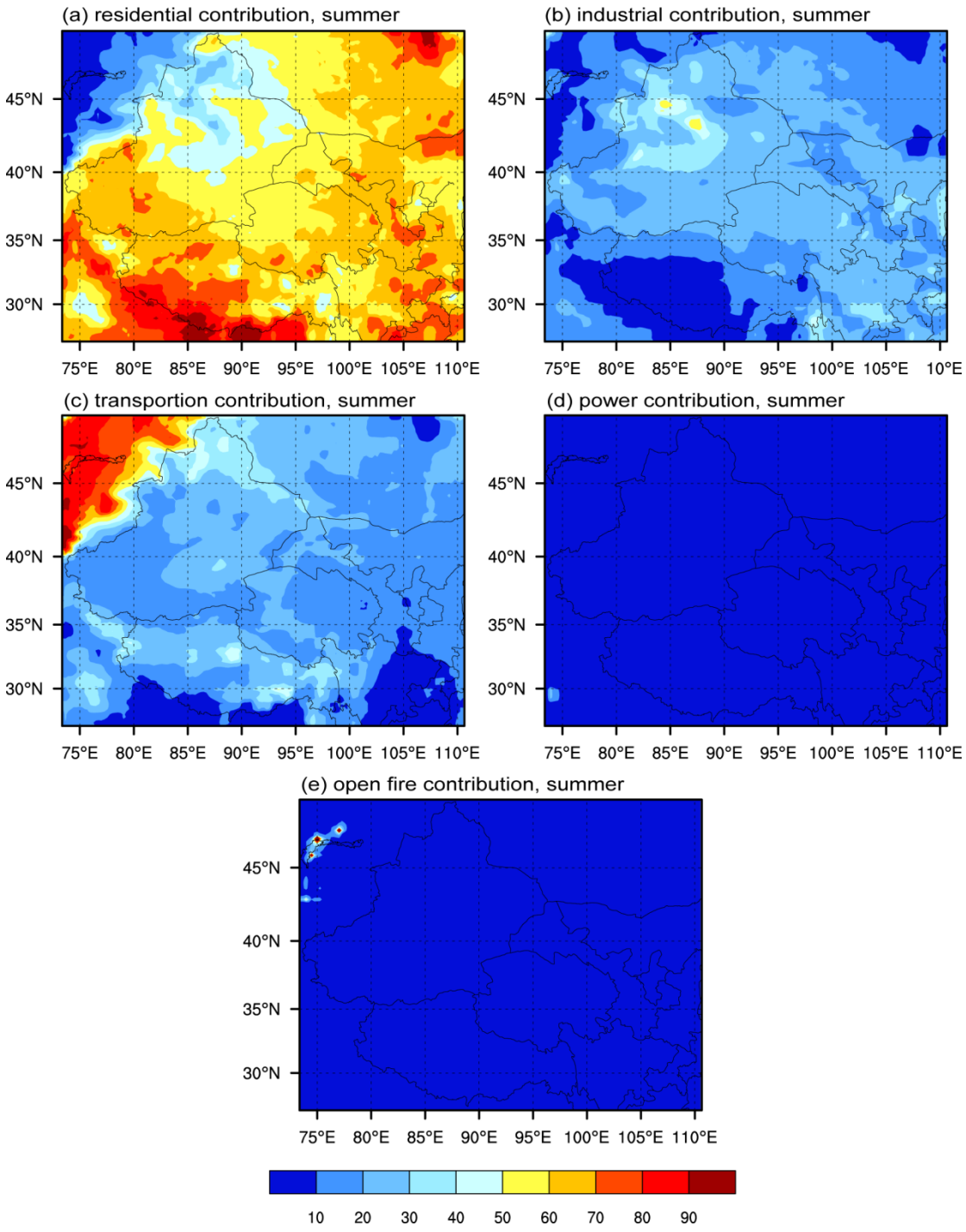

Fig. 10 Contribution ratios (%) from each individual source to the summer mean

simulated BC concentrations: (a) residential, (b) industry, (c) transportation, (d) power, and (e) open fire.

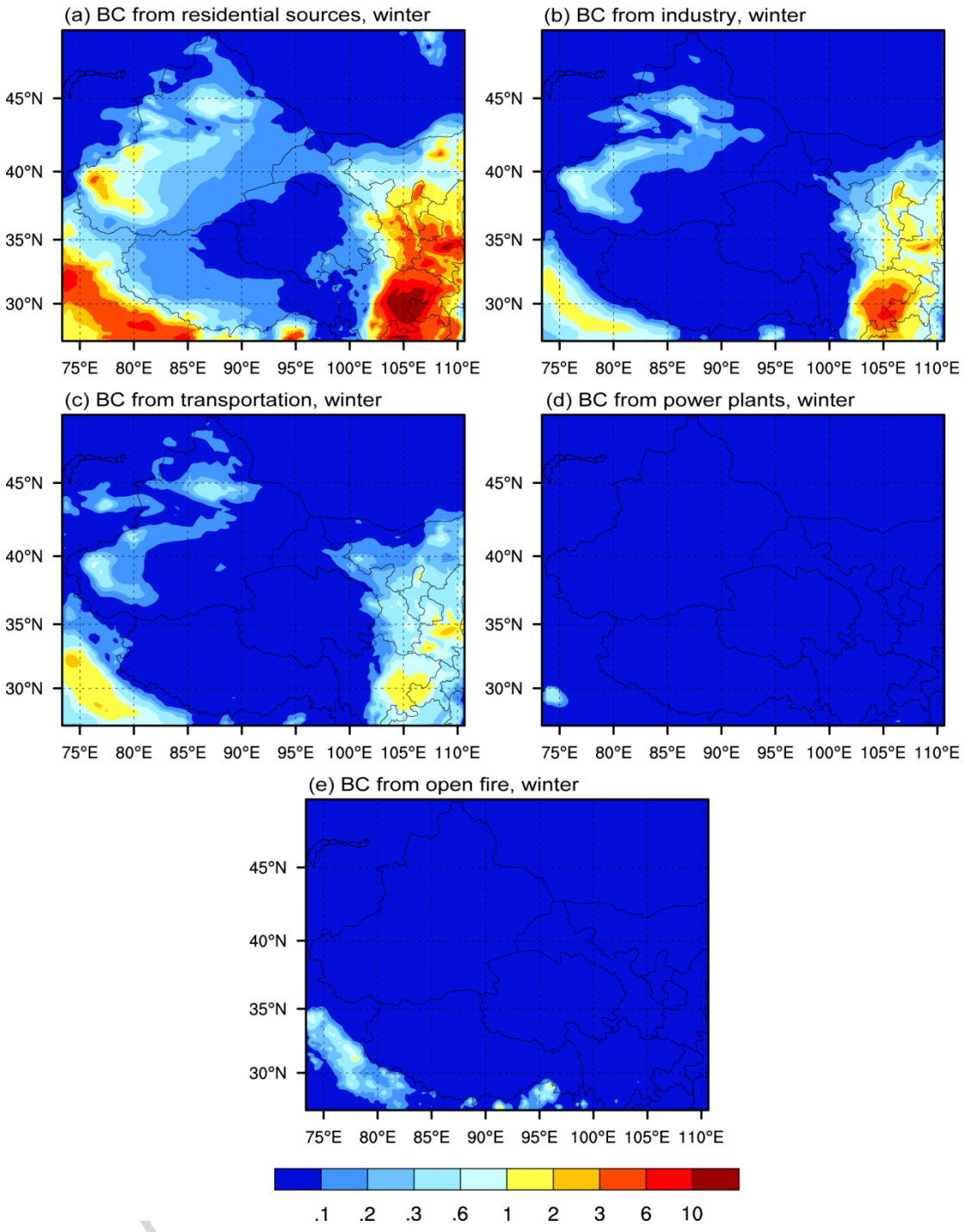

Fig. 11 Average winter BC concentration (μg m^{-3}) from total source and each individual source: (a) residential, (b) industry, (c) transportation, (d) power, and (e) open fire.

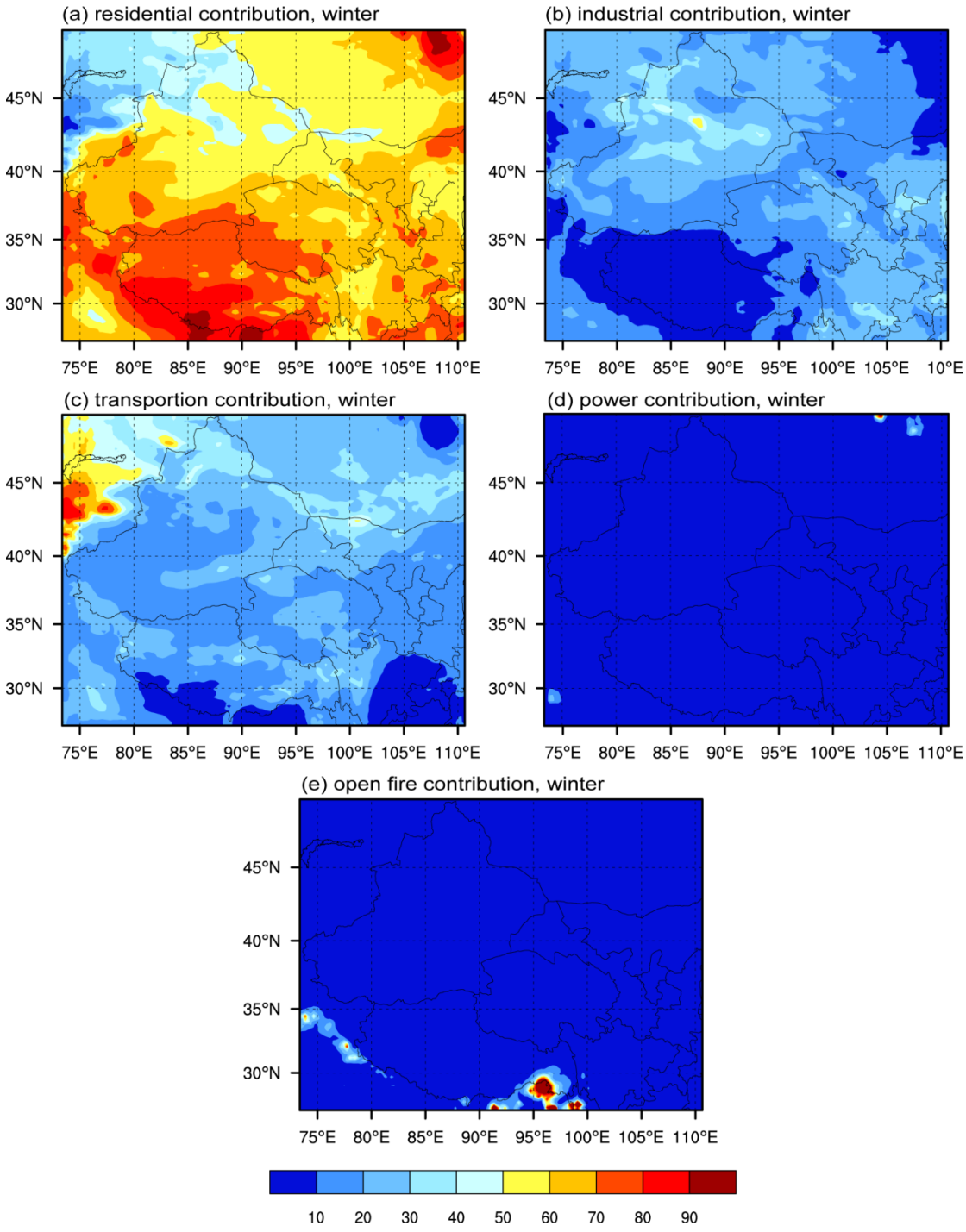

Fig. 12 Contribution ratios (%) from each individual source to the winter mean simulated BC concentrations: (a) residential, (b) industry, (c) transportation, (d) power,

and (e) open fire.

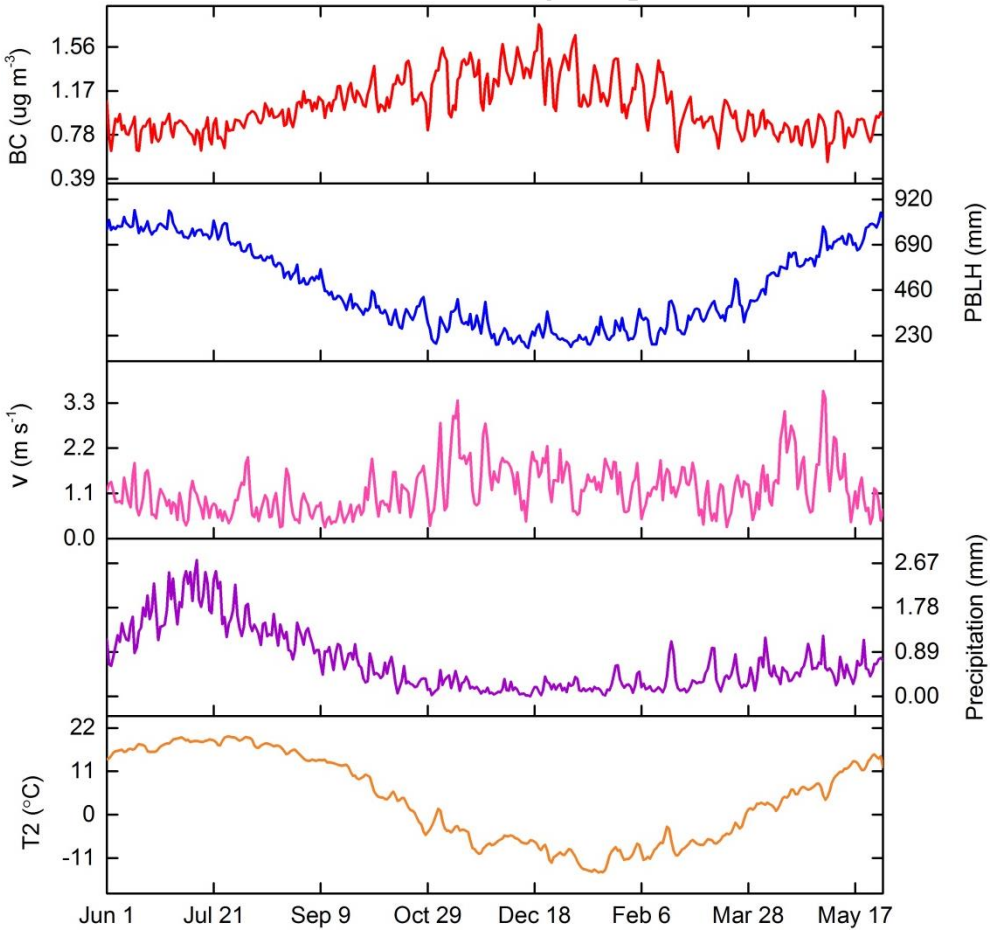

Fig. 13 Variations of simulated BC concentrations, boundary layer height (PBLH), surface wind speed (V), precipitation and 2-m temperature (T2) averaged in western China form June 2016 to May 2017.

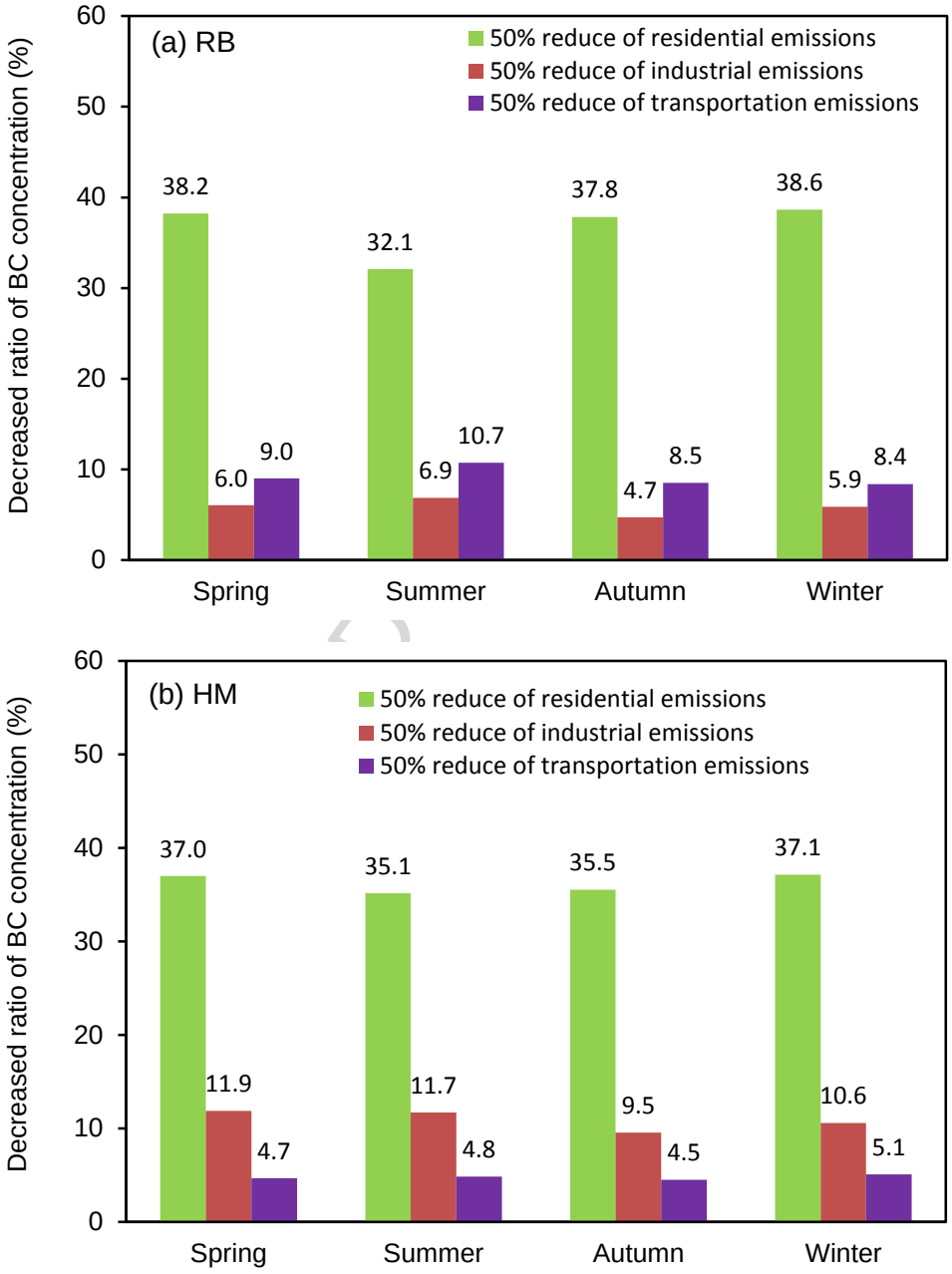

Fig. 14 Decreased ratios of surface BC concentration in RB (a) and HM (b) regions after a 50% reduction of various anthropogenic sources.

Highlights

- The residential emission sector presented the largest contribution to the annual mean BC concentrations.
- Increased BC concentrations in winter were resulted from residential winter heating and poor diffusion and diluted conditions
- Except for residential emission, the transportion sources also should be paid attention when designing control strategies for air pollution over the TP